Pressure and Temperature Dependence of the Gas-Phase Reaction of SO_3 with H_2O and the Heterogeneous Reaction of SO_3 with H_2O/H_2SO_4 Surfaces

John T. Jayne,[†] Ulrich Pöschl,[‡] Yu-min Chen,[‡] David Dai,[‡] Luisa T. Molina,[‡] Douglas R. Worsnop,[†] Charles E. Kolb,[†] and Mario J. Molina*[,‡]

Center for Chemical and Environmental Physics, Aerodyne Research, Inc., Billerica, Massachusetts 01821-3976, and Department of Chemistry and Department of Earth, Atmospheric and Planetary Sciences, Massachusetts Institute of Technology, Cambridge, Massachusetts 02139-4307

Received: August 4, 1997; In Final Form: October 10, 1997[⊗]

The gas-phase reaction of SO_3 with H_2O and the heterogeneous reaction of SO_3 with $H_2O-H_2SO_4$ surfaces have been studied in a fast flow reactor coupled to a chemical ionization mass spectrometer (CIMS) for species detection. The gas-phase reaction was studied under turbulent flow conditions over the pressure range from 100 to 760 Torr N_2 and the temperature range from 283 to 370 K. The loss rate of SO_3 was measured under pseudo-first-order conditions; it exhibits a second-order dependence on water vapor concentration and has a strong negative temperature dependence. The first-order rate coefficient for the SO_3 loss by gas-phase reaction shows no significant pressure dependence and can be expressed as $k^I(s^{-1}) = 3.90 \times 10^{-41} \exp(6830.6/T)[H_2O]^2$ where $[H_2O]$ is in units of molecule cm^{-3} and T is in Kelvin. The overall uncertainty of our experimentally determined rate coefficients is estimated to be ±20%. At sufficiently low SO_3 concentrations ($<10^{12}$ molecule cm^{-3}) the rate coefficient is independent of the initial SO_3 level, as expected for a gas-phase reaction mechanism involving one SO_3 and two H_2O molecules. However, at higher concentrations and lower temperatures, increased rate coefficients were observed, indicating a fast heterogeneous reaction after the onset of binary homogeneous nucleation of acid hydrate clusters leading to particle formation, which was verified by light-scattering experiments. The heterogeneous loss of SO_3 to the reactor walls has also been investigated under low pressure (1.1−12.5 Torr) laminar flow conditions. The loss rate is highly dependent on the humidity of the surface. In the presence of excess water the reactive sticking coefficient approaches unity and the wall loss rate is gas diffusion limited; under dry conditions it approaches zero, as expected. The atmospheric implications of the homogeneous and heterogeneous SO_3−water reaction are discussed.

Introduction

The reaction between gaseous sulfur trioxide (SO_3) and water vapor produces sulfuric acid vapor and is an important step in the production of new sulfuric acid aerosol in the Earth's atmosphere.[1,2] New particles can form by binary homogeneous and heterogeneous nucleation involving H_2SO_4 hydrates. The condensation of sulfuric acid vapor on preexisting particles as well as the heterogeneous reaction of SO_3 with aqueous acid droplets leads to particle growth. In the high-latitude stratosphere sulfate aerosols are known to catalyze ozone destruction.[3,4] These particles can also influence climate directly through scattering of solar radiation and indirectly by acting as cloud condensation nuclei.[5] Background sulfate aerosol levels in the atmosphere can be perturbed by the release of sulfur gases, predominantly SO_2, which is oxidized to SO_3 in the gas phase by the mechanism proposed by Stockwell and Calvert:[2]

$$SO_2 + OH + M \rightarrow HSO_3 + M \quad \text{(R1)}$$

$$HSO_3 + O_2 \rightarrow SO_3 + HO_2 \quad \text{(R2)}$$

$$SO_3 + H_2O \rightarrow\rightarrow H_2SO_4 \quad \text{(R3)}$$

Processes such as volcanic eruptions, biogenic activity, and fossil fuel combustion all contribute to the emission of sulfur gases into the atmosphere. Additionally, local enhancements in sulfate aerosol loading can result from operation of commercial aircraft.[6,7] This may be especially important in the stratosphere if the proposed fleet of high-speed civil transport (HSCT) aircraft is employed. In addition to the SO_3 that is formed via reactions R1 and R2 there is also some evidence that gaseous SO_3 can be formed directly by atmospheric oxidation of biogenically produced, reduced sulfur compounds.[8,9] The degree to which atmospheric SO_3 reacts homogeneously with water vapor, rather than heterogeneously with condensed water in aerosols, cloud droplets, or other particulate matter, is critical in determining the rates of new particle formation in the atmosphere.

The goal of the work presented here is to provide accurate reaction rate parameter data for reaction R3 so that the details of the gas-phase SO_x oxidation and sulfuric acid formation in both high-altitude aircraft exhaust plumes and the background atmosphere can be modeled with greater reliability. The results also contribute to the ongoing effort to reveal the mechanism of reaction R3 and provide new insights into the heterogeneous processes competing with reaction R3.

Experimental investigations on the kinetics of the gas-phase reaction of SO_3 with water vapor have had a long history. The first reported kinetics experiment appeared in the literature in 1937 by Goodeve et al.[10] who discussed a complex reaction that ultimately produces sulfuric acid. Since then there have been a number of more recent studies aimed at unraveling the mechanism. In 1975 Castleman and co-workers[1] reported a

* To whom correspondence should be addressed.
† Aerodyne Research, Inc.
‡ Massachusetts Institute of Technology.
⊗ Abstract published in *Advance ACS Abstracts,* November 15, 1997.

S1089-5639(97)02549-8 CCC: $14.00

rather fast bimolecular reaction rate coefficient of 9×10^{-13} cm^3 $molecule^{-1}$ s^{-1} measured in a low-pressure (1.0−1.3 Torr) flow reactor. On the basis of calculations in 1978, Holland and Castleman[11] suggested that SO_3 forms a complex with H_2O, which then rapidly isomerizes to form sulfuric acid via the following mechanism:

$$SO_3 + H_2O + M \leftrightarrow SO_3 \cdot H_2O + M \quad \text{(R4)}$$

$$SO_3 \cdot H_2O \rightarrow H_2SO_4 \quad \text{(R5)}$$

A subsequent theoretical study performed in 1985 by Chen and Moore-Plummer[12] indicated that the direct reaction between SO_3 and H_2O to form H_2SO_4 is unlikely to occur because of a large (∼22 kcal mol^{-1}) transition-state energy barrier. In light of this result Wang et al.[13] performed a low-pressure (∼2 Torr) experiment and reported a significantly lower bimolecular rate constant (5.8×10^{-15} cm^3 $molecule^{-1}$ s^{-1}). The Wang et al. study identified an efficient heterogeneous reaction of SO_3 occurring on the reactor walls. They speculated the heterogeneous reaction may have influenced the Castleman result and qualified their reported rate as being an upper limit to the true gas-phase rate.

In 1993 Reiner and Arnold[14] measured the reaction at 85 Torr, reporting a bimolecular rate constant of 2.4×10^{-15} cm^3 $molecule^{-1}$ s^{-1}, and in 1994[15] they updated the rate constant to a mean value of 1.2×10^{-15} cm^3 $molecule^{-1}$ s^{-1} with no significant pressure dependence over the range ∼24−190 Torr N_2. In 1994 a higher level ab initio study was performed by Hofmann and Schleyer[16] confirming the calculations of Chen and Moore-Plummer[12] that the direct reaction R3 is unlikely. All of these earlier reported experimental studies analyzed the results in terms of reaction R3 or R4 and R5.

In 1994 we reported our initial investigation of this system, which showed that the homogeneous gas-phase reaction mechanism involves two water molecules, not one as suggested by earlier studies, and that the reaction exhibits a strong, negative temperature dependence.[17] These results are qualitatively consistent with a mechanism possibly involving a water dimer and/or an $SO_3 \cdot H_2O$ adduct:

$$SO_3 + H_2O \cdot H_2O \rightarrow H_2SO_4 + H_2O \quad \text{(R6a)}$$

$$\rightarrow SO_3 \cdot H_2O + H_2O \quad \text{(R6b)}$$

$$H_2O + SO_3 \cdot H_2O \rightarrow H_2SO_4 + H_2O \quad \text{(R7a)}$$

$$\rightarrow H_2O \cdot SO_3 + H_2O \quad \text{(R7b)}$$

Note that reactions 6b and 7b represent simple metathetical switching reactions where an adduct water molecule exchanges one hydrogen-bonded partner for another; reaction 6b is exothermic, while reaction 7b, which simply exchanges water molecules, is thermoneutral. Our initial results indicating the involvement of two water molecules stimulated yet another high-level calculation performed by Morokuma and Muguruma,[18] who were the first to consider the importance of a second water molecule in molecular orbital calculations. The Morokuma and Muguruma study indicated that reaction R6a has a negligible barrier to form the acid product and that reaction R7 has a small (∼5 kcal/mol) transition-state barrier and that both reactions proceed through the same six-centered transition-state complex.

Bondybey and English,[19] on the basis of their study of the reaction of SO_3 with water in a neon matrix at 5 K, were the first to suggest that this reaction involves two water molecules.

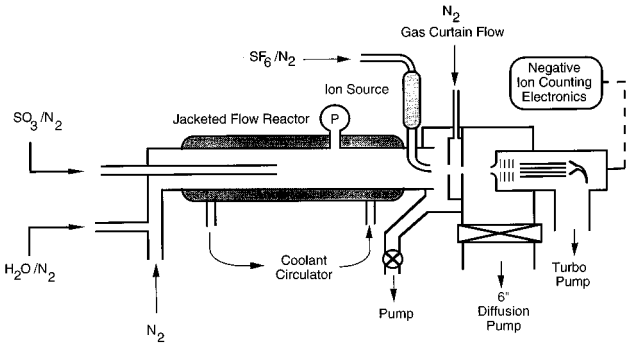

Figure 1. Schematic of the flow reactor coupled to the chemical ionization mass spectrometer used for the study of the gas-phase reaction of SO_3 and water vapor and for the study of the heterogeneous reactivity of SO_3 with aqueous H_2SO_4 surfaces.

These authors also monitored the presence of the $SO_3 \cdot H_2O$ adduct in the matrix. The existence of the $SO_3 \cdot H_2O$ adduct in the gas phase has been verified in a microwave spectroscopy beam experiment.[20] A recent kinetics study by Lovejoy et al.[21] invokes the reaction of the $SO_3 \cdot H_2O$ adduct with water vapor (via reactions R4 and R7a) as the mechanism by which H_2SO_4 is formed. The Lovejoy et al. study reported a strong negative temperature dependence (about −13 kcal/mol), a significant H−D isotope effect, and no apparent pressure dependence over the range 20−80 Torr N_2 at 300 K.

The work reported here extends our previous measurements[17] over the pressure range 100−760 Torr N_2, with temperature dependencies measured at 200, 400, and 760 Torr. In addition, we have performed a separate study to determine the heterogeneous loss rate of SO_3 on the reactor walls to assess its impact on our measurements and to determine the reactive uptake coefficient of SO_3 on H_2SO_4−H_2O surfaces. Rate coefficients were obtained at temperatures between 283 and 370 K; the initial concentration of SO_3 and the water vapor concentration were also varied. At low initial SO_3 concentrations ($<10^{12}$ cm^{-3}) and temperatures above 283 K the measured first-order loss rate of SO_3 is independent of initial SO_3 levels. However, at higher concentrations and lower reaction temperatures, increased reaction rates were observed, most likely due to the onset of binary homogeneous nucleation of acid hydrate clusters ultimately leading to particle formation. The rate constants reported in this paper for the homogeneous gas-phase reaction were measured over the range of conditions for which the reaction rate was observed to be independent of the initial SO_3 level.

Experimental Section

The kinetics experiments were performed in a flow-tube reactor coupled to a chemical ionization mass spectrometer for gas detection; the apparatus is shown schematically in Figure 1. The flow reactor is a Pyrex glass tube, 2.2 cm i.d. and 100 cm in length. The rate measurements for the gas-phase reaction were conducted in the turbulent flow regime with Reynolds numbers in the range 3000−5000 and under pseudo-first-order conditions with water vapor in excess. Sulfur trioxide, as the limiting reagent, was introduced into the flow reactor through a central movable injector. A large flow (∼42 SLPM (standard liter per min)) of dry nitrogen, from a liquid nitrogen gas pack, was used as the main carrier gas. All flows were monitored with calibrated electronic mass flow meters (Tylan General, Matheson Gas Co.). The reactor pressure was monitored by a 1000 Torr pressure gauge (MKS Baratron). At atmospheric pressure the reactor effluent was vented into an exhaust line; lower pressures were achieved with a 1600 L min^{-1} rotary pump (Edwards EM280) controlled by a throttle valve at the reactor

outlet. Temperatures were measured by copper−constantan thermocouples (Omega Engineering). All electronic signals were monitored and processed via a PC-based data acquisition system.

A key feature of the turbulent flow reactor is its "near wall-less" behavior. In turbulent flow a laminar sublayer exists near the wall where the gas velocity approaches zero at the wall. The radial velocity profile of the turbulent core is, to a good approximation, flat and mixing in this regime is achieved by eddy diffusion. Since the flow system is operated at pressures where the rate of molecular diffusion is slow compared to the core velocity, gas transport through the laminar sublayer to the walls is greatly reduced relative to gas transport in low-pressure laminar flow where traditional fast flow reactors are operated. The importance of separating heterogeneous processes from the gas-phase reaction of $SO_3 + H_2O$ had been demonstrated by the earlier results of Wang et al.[13] Our turbulent flow method experimentally allows this separation, while the influence of wall loss and molecular diffusion in laminar flow methods generally demands considerable corrections of the measured loss rate to extract the reaction rate. Furthermore, it is experimentally difficult to achieve fully developed laminar flow except at very low pressures. The ability to perform controlled reaction kinetics using the turbulent flow approach has been demonstrated in our earlier work performed at MIT.[22−24]

Water vapor was introduced at the entrance of the reactor by controlling the flow of N_2 carrier gas through a water bubbler immersed in a water bath to stabilize the temperature. To dilute the saturated water carrier flow, an additional N_2 flow (∼5 SLPM) was added at the outlet of the bubbler. The temperature of the water inside the bubbler was continuously monitored by a thermocouple immersed in the liquid water sample. The water vapor concentration in the flow reactor was controlled in the range $10^{13}-10^{16}$ molecule cm^{-3}. It was calculated from the measured liquid water temperature, the bubbler pressure (measured with a 0−1000 Torr MKS Baratron), the reactor pressure, and the gas flow rates.[25]

The assumption that the N_2 flow leaving the bubbler was saturated with water vapor was verified by two independent experiments. First, the absolute amount of water vapor in the bubbler effluent was monitored by flowing the effluent through a molecular sieve trap held at liquid nitrogen (LN_2) temperature and by measuring the mass increase using an analytical balance. Second, the linearity of the water vapor signal as a function of the N_2 flow through the bubbler was verified by monitoring H_2O^+ at $m/e = 18$ with the mass spectrometer configured in the electron impact ionization mode.

Sulfur trioxide was introduced into the reactor through the movable injector by flowing N_2 (10−100 SCCM (standard cubic centimeter per min)) over the solid SO_3 sample (99.5%, stabilized, Aldrich Chemical, Co), which was contained in a 500 mL glass flask with a gas inlet tube and Teflon stopcocks. The reaction time was controlled by setting the injector at different axial positions. A six-arm spider-shaped Teflon header with four holes on each arm was placed at the end of the injector to facilitate uniform injection throughout the cross section of the tube. In addition a fan-shaped Teflon device was placed immediately behind the header to enhance turbulent mixing. This arrangement gave optimum mixing distances as short as 5 cm, which was confirmed in a separate series of experiments by injecting an inert tracer.[24] The SO_3 sample was held at temperatures between 208 and 223 K in a cooling bath (Syltherm XLT, Dow Corning) refrigerated by a copper coil connected to a circulating cooler (Neslab ULT 80). At the outlet of the SO_3 container an additional N_2 gas flow (∼4 SLPM) was added to carry the SO_3 vapor through the injector into the reactor. Before mixing with SO_3, both the N_2 flowing through the flask and the additional carrier flow N_2 were dried by passing them through molecular sieve traps (4 Å) immersed in a LN_2 bath.

Sulfur trioxide exists in three solid modifications: α-SO_3 (mp, 335 K), β-SO_3 (mp, 306 K), and γ-SO_3 (mp, 290 K). γ-SO_3 consists of annular trimers. In the presence of trace amounts of water it converts to β-SO_3, which is thought to be a chainlike polymer with water saturation at the chain ends (polysulfuric acid). Owing to the forming of cross-links, unstabilized β-SO_3 further converts to the thermodynamically most stable modification, α-SO_3. The commercially available SO_3 samples used here contain a stabilizer (0.5%) inhibiting polymerization and most likely consist of a mixture of β-SO_3 and α-SO_3. The natural assumption that the latter governs the SO_3 vapor pressure of our sample was verified by a series of acid−base titration experiments. A known flow of N_2 passed through the sample flask, and the amount of SO_3 exiting the flask was titrated by passing the effluent through a gas disperser (20 μm) immersed in a standardized solution of NaOH (0.01 N) with bromothymol blue used as a pH indicator. These measurements were performed over the sample temperature range 223−243 K and agreed to within 20% with the analytical expression for the vapor pressure of the β-modification[26]

$$p_v(\text{Torr}) = \exp(28.9239 - 7000T^{-1})$$

Using this expression, we were able to estimate the SO_3 concentration in the flow reactor, which was controlled between 10^{10} and 10^{14} molecule cm^{-3}.

SO_3 and H_2SO_4 were detected as negative ions after undergoing specific ion−molecule or charge-transfer reactions. Chemical ionization was initiated by injecting either SF_6^- or thermal electrons at the downstream end of the flow reactor. The following reactions were used to detect the sulfur species:

$$SO_3 + SF_6^- \rightarrow SO_3F^- + SF_5$$

$$H_2SO_4 + SF_6^- \rightarrow HSO_4^- + SF_6(H)$$

$$SO_3 + e^- \rightarrow SO_3^-$$

$$H_2SO_4 + e^- \rightarrow HSO_4^- + H$$

Both reactions involving SO_3 are fast and have been separately investigated.[27,28] The reactions involving H_2SO_4 are also expected to be fast, occurring at the gas collision limit.[29] The identities of the neutral products are not known.

SF_6^- ions were generated by passing neutral SF_6 (∼0.05 SCCM) in a flow of N_2 (∼10 SLPM) over either a corona discharge or a radioactive polonium source (^{210}Po, NRD, Inc. Model P2021). Thermal electrons were produced by operating the corona discharge in N_2 (in the absence of SF_6). The ions/electrons were injected into the center of the reactor at the exit end of the flow-tube through a $^1/_4$ in. diameter stainless steel tube at a distance of 2−5 cm from the sampling orifice, allowing ion−molecule reaction times of a few milliseconds. When the polonium source was used, a variable voltage was applied to the steel tube to optimize measured ion intensities (−200 to −500 V depending on the pressure of the flow reactor and the geometry of the ion−molecule reaction region). To generate the corona discharge, a stainless steel needle was inserted into the $^1/_4$ in. tube and shielded from it by a small diameter glass tube. The needle was held at −3 to −4 kV relative to the grounded steel tube, and the discharge current was limited to

about $-20\ \mu$A by a 100 MΩ resistor. The needle was shielded from the reactor gas by a ∼4 cm glass sleeve that was placed over the $^1/_4$ in. stainless steel ion tube. The length of the stainless steel and glass tubes determined the ion−molecule reaction distance, which was 1−2 cm.

Both chemical ionization schemes yielded the same results within experimental uncertainty. The polonium source produces a very stable ion current from 1 Torr to atmospheric pressure and was used for most kinetic measurements reported here. The corona discharge is more sensitive to pressure and flow conditions (operating better at higher pressures), and owing to instabilities in the discharge current, it was not used for the low-pressure work.

Linear detection of SO_3 over the concentration ranges used in our experiments was verified by monitoring the ion signal as a function of N_2 carrier flow through the sample flask in the absence of water vapor. During the kinetic measurements utilizing SF_6^- as the reagent ion, the ratio of its intensity relative to the initial SO_3F^- ion intensity was always greater than 10. The SO_3F^- ion signal detected at $m/e = 99$ was corrected for the background mass interference originating from the S^{34} (4% abundance) and O^{18} (0.2% abundance) isotopes present in HSO_4^-. For large SO_3 depletions (i.e., large H_2SO_4 production) this correction was as much as 30% of the SO_3F^- ion signal. No background signal corrections were applied when the experiments were conducted using electron attachment for which SO_3 was detected as SO_3^- at $m/e = 80$. We have no information to discount the possibility that SO_3 and the possible intermediate $SO_3{\cdot}H_2O$ might be detected as the same product ion by our CIMS detection scheme. However, since the results reported later indicate that the adduct formation occurs on a much faster time scale than the H_2SO_4 formation and is not the rate-limiting step of the reaction, the observed first-order rate constant is not affected by the detection or nondetection of $SO_3{\cdot}H_2O$.

Ions were detected using a quadrupole mass spectrometer (Extrel C50) housed in a two-stage differentially pumped vacuum system. The chamber that houses the mass spectrometer is pumped by a 400 L/s turbopump, and the first-stage vacuum chamber is pumped by a 6 in. diffusion pump. The two chambers are separated by a 1.2 mm i.d. skimmer cone. The operating pressures were roughly $10^{-4}-10^{-5}$ Torr and $10^{-6}-10^{-7}$ Torr for the first and second stages, respectively, varying with the reactor pressure. The ions from the downstream end of the flow reactor were sampled through a 50 μm orifice held at −120 V. An einzel lens assembly was mounted between the two apertures and helped focus the ion beam in the first vacuum chamber. The skimmer cone at the entrance to the quadrupole chamber was charged to about +400 V.

Since the water vapor levels in these experiments were appreciable, partitioning of the negative ions to ion hydrates occurred to a noticeable extent (formation of $SO_3F^-{\cdot}(H_2O)_n$, etc.). To investigate any potential influence on the detection scheme, some experiments were conducted with a dry gas curtain installed at the high-pressure side of the sampling orifice. The annular gas outlet (see Figure 1) was positioned around the orifice, and dry N_2 (∼2 SLPM) flowed counter to the main gas flow such that the sampled ions had to penetrate a region where the humidity was much lower than throughout the flow reactor. With the gas curtain operating, the intensity of the hydrate ion peaks could be reduced by ∼95%. The reduction of hydrate partitioning by the gas curtain did not affect the observed SO_3 decay rates.

As an additional test of our detection scheme, some of the kinetics experiments at 760 Torr were performed by sampling a small fraction of the reactor flow into a separately pumped ion−molecule flow-tube operated at 200 Torr. The results of the measurements performed with this experimental configuration showed no significant deviation from the results we obtained in the usual configuration without a separate ion−molecule flow tube.

The temperature of the reactor gas was measured at the entrance and exit using calibrated iron−constantan thermocouples. Under turbulent flow conditions the temperature regulation of the reactor involves precooling (or preheating) the main carrier gas as well as regulating the temperature of the flow reactor itself. For the measurements performed above room temperature, the main nitrogen carrier gas and the flow reactor were resistively heated and the flow reactor was wrapped with reflective insulating material. Below room temperature, a jacketed glass flow reactor was used with a nonflammable coolant (Syltherm XLT, Dow Corning) chilled by a circulating cooler (Neslab LT 50). For these studies the carrier gas was precooled by passing it through a $^3/_8$ in. diameter copper coil (6 m) immersed in an ice−water bath followed by resistive heating. The axial temperature gradient, as measured by the thermocouples placed at the inlet and exit of the flow reactor, was controlled to within 1 K.

The wall loss experiments performed under laminar flow conditions at 1.1−12.5 Torr were conducted with the same experimental setup. The main difference was the use of smaller gas flows (total flow < 1 SLPM, Reynolds number < 50) and a larger sampling orifice (250 μm). The reactor pressure was monitored by a 0−10 Torr MKS Baratron pressure gauge, and the pressure inside the bubbler was separately regulated between 300 and 700 Torr.

Results

Homogeneous Gas-Phase Reaction. Experimental runs were performed by recording the SO_3 concentration at the exit end of the reactor as a function of reaction distance for fixed water vapor concentrations. Typical data sets for a series of water concentrations in the range $10^{15}-10^{16}$ molecules cm^{-3} are displayed on semilog plots with linear fits shown in Figure 2. The data in Figure 2a were obtained with the gas curtain installed on the apparatus using electron attachment detection. The data in Figure 2b were obtained with SF_6^- detection and without the gas curtain, yielding equivalent decay rates. Note, however, that the SO_3F^- signal levels decreased with each successive increase in the water vapor concentration. Hydrate ion partitioning led to the lack of a common intercept at zero reaction distance. Rate coefficients for the measured SO_3 loss, k_{obs}, are obtained as the negative slope of linear fits such as the ones shown in Figure 2, assuming pseudo-first-order conditions ($H_2O \gg SO_3$) and a reaction time that is linearly related to the reaction distance.

Under turbulent flow conditions the appropriate gas velocity to convert reaction distance to reaction time is not the bulk velocity given by the total volumetric flow and the geometric cross section of the reactor. The reaction time is determined by the core gas velocity, which is slightly greater than the bulk gas velocity owing to the existence of the boundary layer near the walls. As was shown in our earlier work,[22−24] the ratio of the core velocity, v_c, to the bulk gas velocity, v_b, is a function of the Reynolds number, $v_c/v_b = (1 + 87.8\mathrm{Re}^{-0.768})$; it varies between 1.19 and 1.13 for Reynolds numbers in the range 3000−5000 typical of these experiments (we note that the value $\mathrm{Re}^{-0.768}$ was misprinted in ref 22 as $\mathrm{Re}^{-0.786}$). The effective velocity, which was independently measured using a pitot static velocity probe and studies of pulsed tracer injection, provides

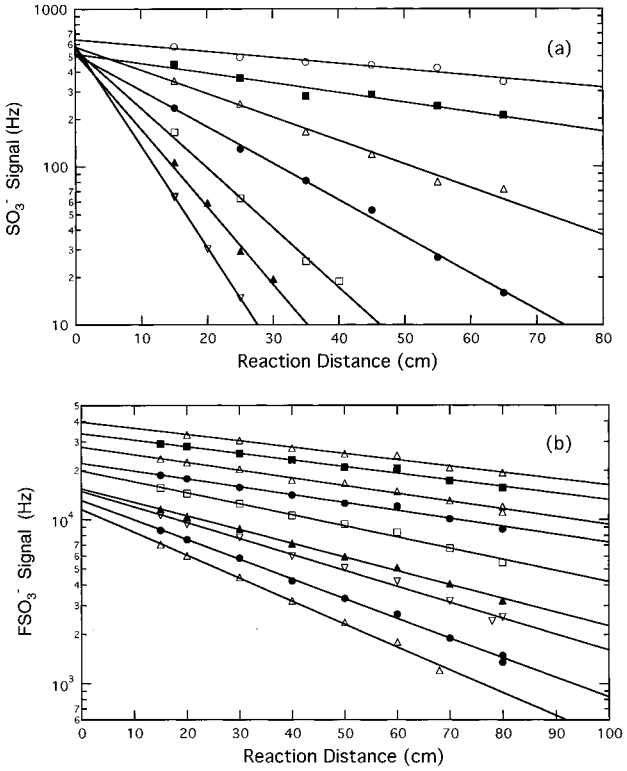

Figure 2. Decay of SO_3 measured as a function of reaction distance for different water vapor concentrations at 302 K: (a) measured at 760 Torr N_2 using $SO_3 + e^-$ detection scheme with gas curtain device active; (b) measured at 100 Torr using $SO_3 + SF_6^-$ detection scheme and no N_2 gas curtain purge (note lack of common intercepts; see text for discussion). Turbulent core gas velocity was 330 cm s^{-1} for the data shown in panel a and 1884 cm s^{-1} for the data shown in panel b.

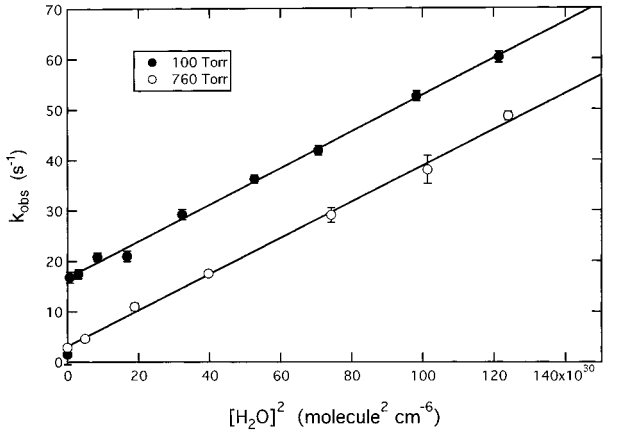

Figure 3. First-order decay rates of SO_3 (from Figure 2) plotted as a function of water vapor concentration: (●) measured at 100 Torr; (○) measured at 760 Torr total pressure. Both data sets exhibit a second-order dependence on water vapor concentration. The solid lines are fits to the data sets that assume a reaction that is second order in H_2O. Also evident is the increased wall loss rate seen in the 100 Torr data (see text for discussion).

an effective measure of the thickness of the boundary layer, which varies between 0.9 mm at Re = 3000 and 0.6 mm at Re = 5000.

In Figure 3 the first-order SO_3 decay rate coefficients obtained from the data sets shown in Figure 2 (100 and 760 Torr, 302 K) are plotted as a function of the square of the water vapor concentration. The figure illustrates the linear dependence of the decay rate on the second power of the water vapor concentration. This was observed for all the data sets across the temperature and pressure ranges investigated, except for very high SO_3 concentrations and low temperatures as discussed later. The solid lines in the plots are linear fits to the data. By use of the expression $k_{obs} = k^{III}[H_2O]^2 + k_w$, a third-order rate coefficient k^{III} with units of molecule^2 cm^6 s^{-1} is obtained. k_w stands for the first-order wall loss rate coefficient. At constant water vapor concentrations, $k^{III}[H_2O]^2$ can be regarded as the first-order rate coefficient for the gas-phase reaction, k^I.

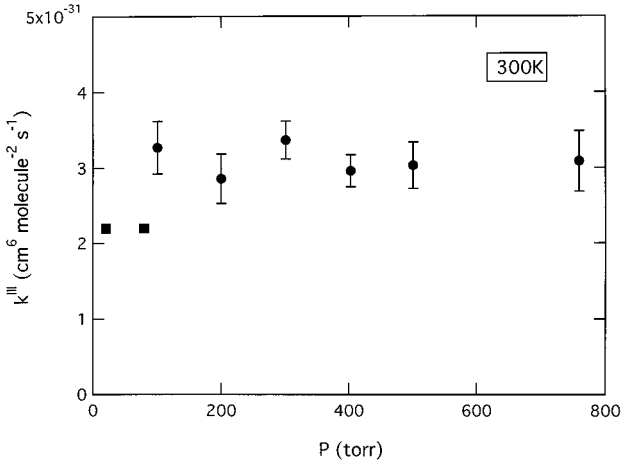

Figure 4. $SO_3 + 2H_2O$ reaction rate coefficient (k^{III} (●)) plotted as a function of total N_2 pressure measured at temperatures between 298 and 302 K. Data have been normalized to 300 K using the measured temperature dependence. Each point represents an average of two to four individual measurements. Error bars are 2σ. Squares are data from ref 21.

The observed overall SO_3 loss rate can be represented by

$$-d[SO_3]/dt = k^{III}[H_2O]^2[SO_3] + k_w[SO_3]$$

and for constant water vapor concentration

$$-d[SO_3]/dt = (k^I + k_w)[SO_3] = k_{obs}[SO_3]$$

The variation in the intercept between the two sets of data in Figure 3 indicates an increased wall loss rate, k_w, at lower pressures. Note also that for the 100 Torr set the fitted line does not include the lowest k_{obs} value shown in the figure. This data point differs from the rest in that the water vapor source was completely shut off. The abrupt decrease in that k_{obs} value relative to its nearest neighboring point implies that the wall loss rate depends on the presence of water. This observation, together with the pressure dependence of k_w, prompted a separate set of experiments to study the wall loss rate and to determine its dependence on water vapor concentration. The results and their implications are discussed in the wall reaction section.

The pressure dependence of the gas-phase reaction was investigated over the range 100−760 Torr N_2 at 300 K. No statistically significant variation was observed in either the absolute rate constant or the second-order dependence on water vapor concentration. This result, plotted in Figure 4, suggests that the formation and equilibration of the dimer $H_2O{\cdot}H_2O$, and/or the adduct $SO_3{\cdot}H_2O$, is not the rate-limiting process governing the overall loss rate of SO_3.

The temperature dependence of the reaction was investigated over the range 283−370 K at three different total pressures, 200, 400, and 760 Torr. Experiments at each pressure yielded essentially the same effective temperature dependence. Despite the complex nature of the reaction, SO_3 loss is well described by the following Arrhenius expression over the experimental temperature range:

$$k^{III} = A \exp\left(-\frac{E_a}{RT}\right) \quad (1)$$

where A is the preexponential factor, E_a is the Arrhenius activation energy, T is the absolute temperature, and R is the gas constant. The data are plotted in Figure 5. The solid line in the figure is the best fit of all the data to eq 1, which yields a value of $A = 3.90 \times 10^{-41}$ cm^6 molecule^{-2} s^{-1} and $E_a = -13.5$ kcal mol^{-1}. Also included in the figure is the temperature dependence reported by Lovejoy et al.,[21] which represents their measurements over the total pressure range from 20 to 80 Torr.

The absolute value of the rate coefficient predicted by our Arrhenius expression for 295 K is 2.7 times smaller than the rate coefficient suggested in our previous publication for 295 K.[17] The focus of that publication was to report on the second-order water vapor concentration dependence, which had been observed for the first time. The discrepancies between the rate coefficients are attributed to calibration uncertainties in the determination of the reactor temperature and water vapor concentrations in those preliminary experiments (both parameters have been very carefully calibrated for this work) as well as an overall refinement of the experimental technique for measuring this reaction.

The sulfuric acid signal (HSO_4^- ion) was also recorded as a function of reaction time for all the experiments in order to determine if H_2SO_4 vapor production was consistent with SO_3 consumption. The production of sulfuric acid vapor as a function of $SO_3 + H_2O$ reaction time was observed to be consistent with the second-order loss of SO_3 vapor. A kinetic model was constructed to analyze these data, which set the production rate of H_2SO_4 equal to the loss rate of SO_3, i.e., $-d[SO_3]/dt = +d[H_2SO_4]/dt$. Two unknown parameters were required to match the model prediction to the data points. These two parameters accounted for the detection efficiency of H_2SO_4 relative to SO_3 and the background signal of H_2SO_4 vapor. The sulfuric acid background was observed to depend strongly both on the temperature of the reactor and on the partial pressure of water vapor present. At temperatures above ~310 K the acid background was about 3 times larger than the vapor produced by the homogeneous reaction and the H_2SO_4 signal was nearly independent of the extent of reaction. At lower reactor temperatures the time dependent production rate of sulfuric acid vapor could be resolved, since the H_2SO_4 signal from the background was ~5 times lower than that produced from the gas phase. Under these conditions the data indicated an additional dependence of the acid vapor background on the concentration of water vapor. Acid background levels decreased as the water vapor concentration increased. To account for this trend, we included in the model an acid vapor background that had a functional dependence on water vapor and temperature based on the parametrization for the vapor pressures of the $H_2SO_4-H_2O$ system given by Taleb et al.[30] Unfortunately, a global fit to all the data was not possible, since the acid vapor background was dependent on the total H_2SO_4 accumulation in the system. The relative CIMS detection efficiency determined from the single fits suggests that $k_{H2SO4} = \sim 2k_{SO3}$ where k is the ion molecule reaction rate with SF_6^-. The results are consistent with the calculated collision-limited rate coefficient for H_2SO_4 with SF_6^- of 1.9×10^{-9} cm^3 molecule^{-1} s^{-1} [29] and previous product studies for the SO_3-water vapor reaction.[21]

Based on the assumption that H_2SO_4 yield is unity ($-d[SO_3]/dt = +d[H_2SO_4]/dt$), the maximum H_2SO_4 gas-phase concentration generated by the reaction should be equivalent to the initial SO_3 concentration under conditions of high reactivity, i.e., high water vapor levels and low temperature. Under these conditions

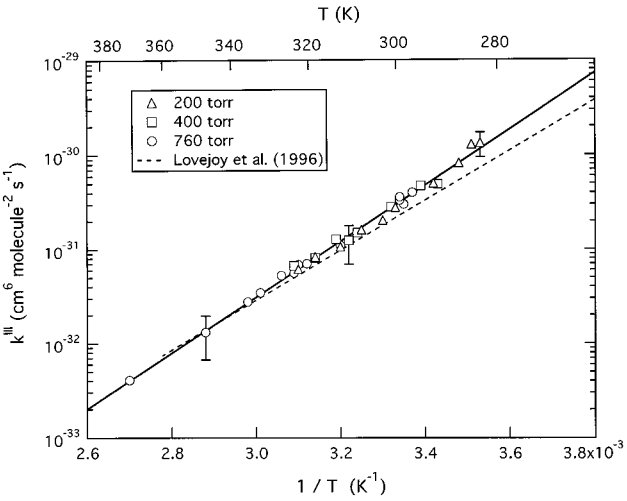

Figure 5. Arrhenius representation of the temperature-dependent reaction rate data measured at 200, 400, and 760 Torr. The best fit to the combined data sets yields an effective temperature dependence of −13.5 kcal mol^{-1}. Dashed line is reproduced from ref 21 (−13.0 kcal mol^{-1}).

secondary reactions of SO_3 with acid hydrates need to be considered. An upper limit to any potential SO_3-acid hydrate reaction rate can be estimated if one assumes that (1) all the initial SO_3 is converted to H_2SO_4, (2) all the acid exists in a reactive hydrate form, and (3) this reaction contributes at the 20% uncertainty level of these experiment ($k_1 \approx 10$ s^{-1}). Taking the acid hydrate concentration to be ~10^{12} cm^{-3}, a rate constant limit of $<10^{-11}$ cm^3 molecules^{-1} s^{-1} is estimated. If there were an efficient reaction of SO_3 with $(H_2SO_4)_x \cdot (H_2O)_y$, we would not have observed consistently a first-order dependence on $[SO_3]$ and a second-order dependence on $[H_2O]$. This suggests that any secondary reactions were not contributing significantly to the measured SO_3 decays. Although the H_2SO_4 level is larger in the absence of water vapor, as discussed above, any potential secondary chemistry is less likely to be observed, since the formation of acid hydrate is not favored.

Wall Reaction. To elucidate the humidity and pressure dependence of the SO_3 wall loss observed under turbulent flow conditions and to validate the data analysis method used to obtain the gas-phase reaction rate constants, additional wall loss measurements were performed under laminar flow conditions at total pressures from 1.1 to 12.5 Torr N_2. By use of the polonium source CIMS detection scheme, SO_3F^- was monitored as a function of injector distance under dry conditions and for water vapor concentrations from 10^{13} to 10^{15} cm^{-3}. No significant wall loss of SO_3 was observed on clean Pyrex glass in the absence of water. Owing to the high vapor pressure of SO_3 at room temperature—more than 10 times the partial pressure in the reactor—no irreversible deposition of SO_3 other than possibly a thin adsorption layer is to be expected on dry glass surfaces. The loss of SO_3 in the reactor due to processes that may occur on a clean glass surface (reaction with trace amounts of surface water and/or OH groups as well as physical adsorption−desorption) was not significant. The loss rates observed under these conditions was around 1 ± 1 s^{-1}. A value of 2 s^{-1} would correspond to $\gamma \approx 10^{-4}$ as an upper limit for the reactive uptake coefficient. When the walls were covered with a coating of aqueous sulfuric acid, the reactive loss of SO_3 was significant. This wall loss decreased within minutes after shutting off the water vapor flow. The observed loss rates and thus the probability for reactive uptake of SO_3 by the sulfuric acid coating on the walls continued to decrease until the vapor pressure of SO_3 over the highly concentrated sulfuric acid

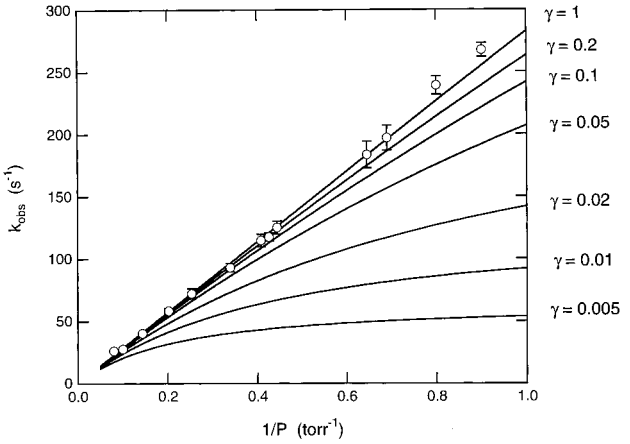

Figure 6. Diffusion-limited loss of SO_3 to reactor wall measured under laminar flow conditions as a function of total N_2 pressure. The lines in the figure refer to predicted wall loss rates for different values of γ. Assuming $\gamma = 1$, a linear fit to the data yields a value of 94.6($\pm$3) Torr cm^2 s^{-1} for the diffusion coefficient of SO_3 in N_2 at 300 K (see eq 2).

($\sim$100%) or oleum reached the partial pressure of SO_3 in the reactor. As expected, experimental runs performed under these conditions showed no significant wall loss. However, a reversible absorption−desorption process was measurable on a time scale of tens of seconds to a few minutes after every change of the SO_3 injector position. When the injector was moved downstream, a temporary increase ($\sim$30 s) of the SO_3F^- signal could be observed while moving the injector upstream resulted in a temporary decrease (2−3 min). These absorption−desorption processes are attributed to the equilibration of the sulfuric acid−oleum coating on the walls with the reactor gas upstream or downstream of the SO_3 injector.

When the water vapor concentration exceeds the SO_3 concentration in the reactor, the loss rate increases to the gas diffusion limit, showing a linear dependence on the inverse of pressure. The diffusion-limited wall loss coefficient, k_w, in a tubular flow reactor can be approximated by[31]

$$k_w = \frac{3.66 D_p}{r^2 P} \qquad (2)$$

where D_p is the pressure-normalized gas-phase diffusion coefficient, r is the reactor radius, and P is the total pressure. This expression is derived for the condition that the concentration of SO_3 at the reactor wall is zero. The wall loss rate was measured as a function of pressure in the 1.1−12.5 Torr range; the data are plotted in Figure 6 versus 1/P. By use of eq 2 with $k_w = k_{obs}$, a linear fit to the data (not shown in the figure) yields a value for a SO_3−N_2 diffusion coefficient of 94.6($\pm$3) Torr cm^2 s^{-1} at 300 K, in agreement with the value of 90 at 300K predicted by the CHEMKIN computer program[32,33] and another experimentally determined value of 87 $\pm$ 8 at 295 K.[34] The lines in the figure model the wall loss rate for the conditions of the experiments for different values of the reaction probability ($\gamma = 1$, 0.2, 0.1, 0.01, and 0.001) and suggest that a value of $\gamma = 1$ best fits the observations.[35] A lower limit of $\gamma = 0.67$ is obtained from a nonlinear best fit through the lower 2σ error bars of the data in Figure 6 using the Brown formalism[35] and keeping the diffusion coefficient value fixed at 94.6. The data shown in Figure 6 represent averages of two to six individual measurements where at a given pressure the amount of water vapor present was also varied from 10^{13} to 2×10^{15} molecules cm^{-3}. The addition of water vapor was neglected in the determination of the gas-phase diffusion coefficient, since in the maximum case [H_2O] accounted for only 5% of the gas mixture. The near unity surface reaction probability measured here seems invariant over a H_2SO_4−H_2O surface composition ranging from 78 to 92 wt % H_2SO_4.

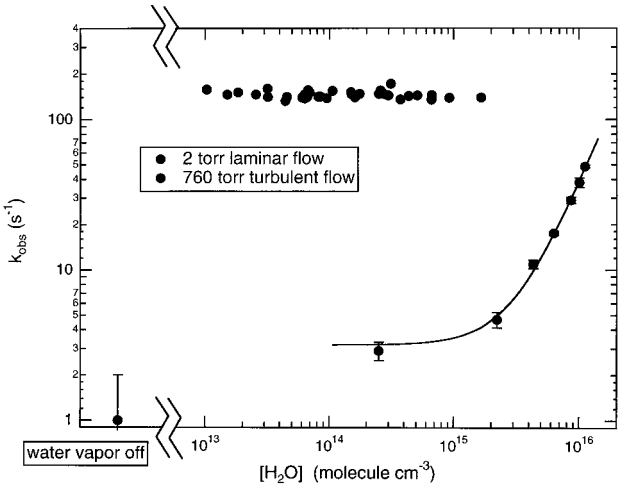

Figure 7. Reactive loss of SO_3 measured at low-pressure laminar flow conditions (solid points) and at turbulent flow conditions (open circles) as a function of water vapor concentration (note break in axis). Low-pressure loss rate is dominated by heterogeneous reaction on reactor walls and is diffusion-limited when trace levels of water vapor are present. Solid points were obtained over the pressure range 1.1−12.5 Torr and have been normalized to 2 Torr for display purposes. In dry reactor (water vapor source off) wall loss is negligible. The observed first-order rate coefficients measured under turbulent flow conditions exhibit a dependence on water vapor concentration that is due to gas-phase reactivity.

As long as the water vapor concentration exceeded the SO_3 concentration, neither the presence of varying amounts of sulfuric acid coating on the walls nor variations of water vapor had a noticeable effect on the loss rate measurements. The full data set from Figure 6 (before averaging data points) is displayed in Figure 7 (solid circles) as a function of water vapor concentration. Since the data were obtained over the pressure range 1.1−12.5 Torr, they have been normalized to 2.0 Torr for display purposes using the observed pressure dependence shown in Figure 6. Also included in Figure 7 is the 760 Torr data set (open circles) replotted from Figure 3, which demonstrates the utility of performing the reaction in the near "wall-less" turbulent flow reactor.

Owing to the difficulties of controlling very low water levels with our experimental setup, we were not able to resolve the onset of significant wall loss. At water concentrations slightly larger than the estimated SO_3 concentration (e.g., [H_2O] = 2×10^{13}, [SO_3] = 1×10^{13}), we still observed diffusion-limited loss rates indicating near unit probability for the reactive uptake coefficient. At water vapor concentrations slightly smaller than the estimated SO_3 concentration (e.g., [H_2O] = 2×10^{13}, [SO_3] = 5×10^{13}), we no longer observed measurable wall loss. The very narrow concentration range in which the transition from negligibly small to unit uptake probability for SO_3 occurs can be explained with the thermodynamic properties of the H_2SO_4−H_2O−SO_3 system. At 298 K the equilibrium vapor pressure of SO_3 changes rapidly from $\sim 8 \times 10^{-8}$ Torr (3×10^9 molecules cm^{-3})[36] over 90 wt % H_2SO_4 (total molar SO_3/H_2O mixing ratio of 0.62), to $\sim 2 \times 10^{-4}$ Torr (8×10^{12} molecules cm^{-3}) over 100% H_2SO_4, and to $\sim 2 \times 10^{-3}$ Torr (8×10^{13} molecules cm^{-3})[37] over oleum with 5 wt % excess SO_3 (total molar SO_3/H_2O mixing ratio of 1.07), respectively. Our observations indicate that at SO_3/H_2O mixing ratios close to 1, a rapid heterogeneous reaction with γ for both H_2O and SO_3

close to 1 governs the composition of the wall coating. With one of the reactants in excess, the sulfuric acid or oleum wall coating quickly seems to adopt a composition that is in equilibrium with the partial pressure of the excess reactant. Based on this interpretation, the observations also reconfirm our estimate for the SO_3 concentration in the reactor.

The low-pressure diffusion study demonstrates that over the range of water vapor concentrations used for measuring the homogeneous reaction rate (Figure 3), the heterogeneous loss of SO_3 to the walls occurs with near unit probability and is independent of water vapor concentration within this range. Thus, the increase of k_{obs} with $[H_2O] \gtrsim 10^{15}$ molecules cm^{-3} in the turbulent flow experiments can be entirely attributed to the gas-phase reaction, and the intercept of the linear fits to k_{obs} vs $[H_2O]^2$ corresponds to a wall loss rate k_w. As discussed, the abrupt increase in the wall loss rate observed for the 100 Torr data between $[H_2O] = 0$ and $[H_2O] \approx 10^{15}$ molecules cm^{-3} results from activation of the walls by water. The offset in the intercepts between the 100 and the 760 Torr data set in Figure 3 reflects a wall loss decrease with increasing pressure, which is due to decreasing gas transport rates by molecular diffusion from the turbulent core through the boundary layer to the reactor walls. From 100 to 760 Torr k_w decreases linearly with $1/P$ from ~16 to ~2 s^{-1} and is consistent with gas-phase diffusion.[24]

Acid−Water Aerosol Reaction. The effect of initial SO_3 concentration on the measured rate coefficients was also investigated during the course of this work. The rates reported in Figures 2−5 were independent of SO_3 concentration. Usually the initial concentration was on the order of 10^{11} molecules cm^{-3}. Room-temperature experiments performed at up to 40 times higher SO_3 levels gave the same results. However, at higher SO_3 concentrations and lower temperatures we have observed that the measured loss rate coefficient increases with increasing levels of SO_3 in the flow reactor. In addition, the effect was favored by high total pressures. As pointed out in earlier studies (Kolb et al.,[17] Lovejoy and Hanson,[38] Fried et al.[39]), this reaction will produce submicrometer (and larger) size acid aerosol at low temperature, high total pressure, and high $H_2O-SO_3-H_2SO_4$ concentrations. The mechanism of the acid aerosol formation is not well understood but must begin with the formation of cluster species that then nucleate (probably through a binary heterogeneous process) and grow to larger size particles. In the present study we have observed that the rate of consumption of SO_3 as measured in our reactor is strongly enhanced by selecting the conditions that favor particle formation.

In the lowest temperature range of operation (243−268 K) at SO_3 densities of ~10^{12} cm^{-3} very fast decay rates showed a trend to first-order dependence in water vapor and poor reproducibility. With a Mie scattering chamber in place of the CIMS at the exit end of the flow reactor, particles ($\gtrsim 0.2$ μm) were detected in the presence of water vapor. When the water vapor was shut off, the light-scattering signal diminished. The rapid loss of SO_3 associated with the formation of particles can be explained (as is a first-order dependence on $[H_2O]$) by an efficient heterogeneous reaction between SO_3 and the acid−water particles.

Qualitatively, the SO_3 loss rate coefficient as measured in our reactor falls into one of three categories. First, for low initial reactant concentrations ($SO_3 < 10^{12}$ molecules cm^{-3}) and moderate-to-high temperatures (283−370 K), the pure gas-phase process dominates the measured SO_3 consumption Figures 2−5). For intermediate SO_3 levels at room temperature ($10^{12}-10^{13}$ molecules cm^{-3}) increased loss rate coefficients are favored by high total pressure. In this regime the measurements still exhibit a nonlinear dependence on water vapor concentration, are reproducible, and suggest that both the homogeneous gas-phase reaction and the reaction with gaseous acid hydrates account for the observed loss rates. As the SO_3 level is further increased and/or the temperature is decreased, SO_3 consumption strongly increases to the point where heterogeneous reaction of SO_3 on water acid clusters dominates the loss.

TABLE 1: Thermodynamic Parameters Describing Equilibrium Formation of $H_2O \cdot H_2O$

ΔH (cal mol^{-1})	ΔS (cal mol^{-1} K^{-1})	K_{eq}, 300 K (atm^{-1})	ref
−3590	−18.59	0.036	Curtiss et al.[41]
−3800	−18.52	0.052	Morokuma and Mugurama (private communication)
−4282	−18.21	0.138	Slanina and Crifo[40]

As mentioned before, the SO_3 concentration at which the deviation from the gas-phase homogeneous reaction occurs was observed to be dependent on the total pressure of the reactor. The following numbers refer to room temperature and H_2O densities of ~5×10^{15} molecules cm^{-3}. At 200 Torr, SO_3 dependent loss rate coefficients were measured at SO_3 concentrations larger than ~4×10^{12} molecules cm^{-3}. At 400 Torr the heterogeneous effect became apparent at $[SO_3] > 2 \times 10^{12}$ molecules cm^{-3}, while at 760 Torr it already occurred at $[SO_3] > 1 \times 10^{12}$ molecules cm^{-3}. At 1.1−12.5 Torr no $[SO_3]$ dependence of the measured loss rate coefficients was observed for SO_3 concentrations as high as 10^{14} molecules cm^{-3} as long as the H_2O density exceeded the SO_3 density.

When the reaction conditions strongly favor nucleation and particle growth, the measured SO_3 loss rate occurs rapidly on the 5−200 ms experimental time scale. Subsequent studies are planned to more accurately measure the conditions that govern cluster formation and particle growth and to determine the kinetics of these processes. The influence of SO_3 concentration on the reaction was studied by Lovejoy et al.,[21] but no effect was noted, since they operated at lower SO_3 concentrations (~10^9 cm^{-3}). However, we believe that the reaction on water acid clusters may be responsible for the high SO_3 consumption rate originally measured by Castleman et al.[1]

Discussion

The observed second-order dependence on water vapor concentration and the strong negative temperature dependence associated with R3, the $SO_3 + H_2O$ reaction, suggests the formation of bound intermediates and a complex mechanism. The role of such intermediates in this reaction is apparent from reactions R6a and R7a, involving formation of either the water dimer $H_2O \cdot H_2O$ or the adduct $SO_3 \cdot H_2O$:

$$H_2O + H_2O + M \leftrightarrow H_2O \cdot H_2O + M \qquad \text{(R8)}$$

$$SO_3 + H_2O + M \leftrightarrow SO_3 \cdot H_2O + M \qquad \text{(R9)}$$

On the basis of the lack of pressure dependence of the measured rate coefficient, we expect that these two reactions are essentially at equilibrium. The thermodynamic parameters ΔH and ΔS that characterize the equilibrium constant K_{eq} for the water dimer (reaction R8) have recently been computed by Slanina and Crifo[40] and by Morokuma and Muguruma[18] and have been measured by Curtiss et al.[41] Those values are presented in Table 1. The thermodynamic parameters describing reaction R9, presented in Table 2, have been taken from the ab initio calculations by Morokuma and Muguruma[18] and Hofmann and Schleyer[16] and from the estimates given by Lovejoy et al.[21]

TABLE 2: Thermodynamic Parameters Describing Equilibrium Formation of $SO_3 \cdot H_2O$[a]

ΔH (cal mol^{-1})	ΔS (cal mol^{-1} K^{-1})	K_{eq}, 300 K (atm^{-1})	ref
−8282	−21.55	21.0	Morokuma and Mugurama[18]
−7900	−26.5	0.92	Hofmann and Schleyer[16]
> −13000	−26.5	4717	Lovejoy et al.[21]

[a] The ΔH value by Lovejoy et al. is a lower limit based on the interpretation of their experimental results.

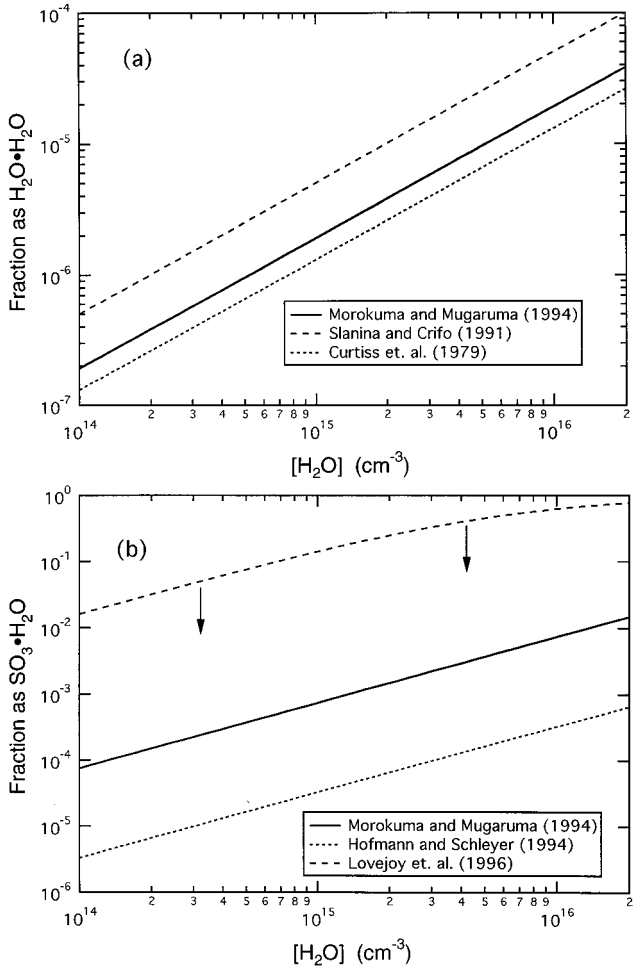

Figure 8. Computed water dimer (a) and $SO_3 \cdot H_2O$ adduct (b) fractions at 300 K as a function of water vapor concentration typically used in these experiments. Lines are from the data in Tables 1 and 2. Dashed line in part b is an upper limit.

based on their interpretation of their own experimental results. The value for a given equilibrium constant is observed to vary widely among these studies, leading to uncertainties in the computed concentration of these intermediate species in our flow reactor as well as in their predicted role in the reaction mechanism. These uncertainties arise in part from difficulties associated with computing the entropy terms for species with internal rotations and/or large amplitude anharmonic vibrations. Such effects have been studied and discussed for the computation of the thermodynamic properties of the water dimer;[42] similar difficulties also exist for the computation of the adduct thermodynamic properties.

Using the data from Table 1, we have plotted in Figure 8 the fraction of water dimer, $[H_2O \cdot H_2O]/([H_2O] + [H_2O \cdot H_2O])$, and adduct, $[SO_3 \cdot H_2O]/([SO_3] + [SO_3 \cdot H_2O])$, that would exist in our flow reactor as a function of water concentration at 300 K under equilibrium conditions. We have assumed that higher hydrates ($(H_2O)_n$, $n > 2$, and $SO_3 \cdot (H_2O)_n$, $n > 1$) are not present to an appreciable extent. The largest amount of $SO_3 \cdot H_2O$ adduct is calculated using the stability limit measured by Lovejoy et al.[21] (see Table 2), predicting 50% of the SO_3 bound as the adduct at 300 K in the presence of 6×10^{15} cm^{-3} [H_2O]. In their low-temperature experiment (252 K) the stability limit predicts that greater than 90% of the SO_3 is in the adduct form with $\sim 10^{14}$ cm^{-3} water vapor concentration.

The data in Figure 8 can be used in conjunction with our experimental measurements to estimate rate coefficients for reactions R6a and R7a. Assuming first that R6a is the sole H_2SO_4-producing reaction and by use of the thermodynamic values of Curtiss et al.[39] for the water dimer, we compute k_{6a}(300 K) $= 2.1 \times 10^{-10}$ cm^3 s^{-1}, which is at or near the collision-limited rate, and we would expect k_{6a} to clearly exceed that limit at lower temperatures. Furthermore, since the reaction most likely proceeds through a six-centered transition state, this fast rate seems unlikely. If reaction R7a is the sole sulfuric acid-producing reaction, using the thermodynamic values for the adduct estimated by Morokuma and Muguruma, we calculate k_{7a} (300 K) $= 1.2 \times 10^{-12}$ cm^3 s^{-1}, which appears more reasonable but which must accommodate a significant activation barrier if the Morokuma and Muguruma calculations are correct[18] (see discussion below).

The values of ΔH for $H_2O \cdot H_2O$ and $SO_3 \cdot H_2O$ shown in Tables 1 and 2 suggest that the water dimer binding energy is $\sim$4 kcal mol^{-1} and the adduct binding energy is $\sim$8 kcal mol^{-1}. Clearly, the magnitude of either of these binding energies can account only partially for the measured activation energy of the overall reaction rate constant (−13.5 kcal mol^{-1}). The difference could be explained by the nature of reactions R6a and R7a, namely, a complex-mode reaction involving the SO_3 dihydrate complex intermediate $(SO_3 \cdot (H_2O)_2)^*$, similar to the one described by Morokuma and Muguruma.[18] Complex-mode reactions often exhibit negative temperature dependencies; in some instances they also display non-Arrhenius behavior and possibly also a pressure dependency.

Out of the observed negative activation energy of −13.5 kcal mol^{-1}, only about 4 or 5 kcal mol^{-1} would need to be accounted for by reaction R7a, if we assume that the overall reaction proceeds through the formation of the SO_3 adduct. The reaction rate for reaction R7a depends on the ratio of the rate of dissociation of the dihydrate intermediate to regenerate the reactants to the rate of the forward reaction to form H_2SO_4. As discussed, for example, by Troe,[43] this ratio depends only on the number of open channels available for the forward reaction compared to the number available for dissociation. This ratio may have a strong negative temperature dependency if the number of open channels for dissociation increases faster with temperature than the corresponding number for the forward reaction. In this case this is precisely what is expected, since the formation of the dihydrate activated complex involves a loose transition state, whereas its decomposition to produce H_2SO_4 proceeds through a tight transition state.

The calculations by Morokuma and Muguruma[18] indicate that the $SO_3 \cdot (H_2O)_2$ dihydrate intermediate is more than $\sim$6 kcal/mol lower in energy than the separate $SO_3 \cdot H_2O$ and H_2O fragments. On the other hand, calculations by these authors also indicate that the six-center transition state for reaction R7a, to form H_2SO_4, is $\sim$5 kcal/mol higher in energy than the $SO_3 \cdot H_2O$ and H_2O reactants. It would be difficult to rationalize the observed overall negative temperature dependency with a complex-mode mechanism involving the SO_3 adduct if such a large activation energy barrier indeed exists. However, the

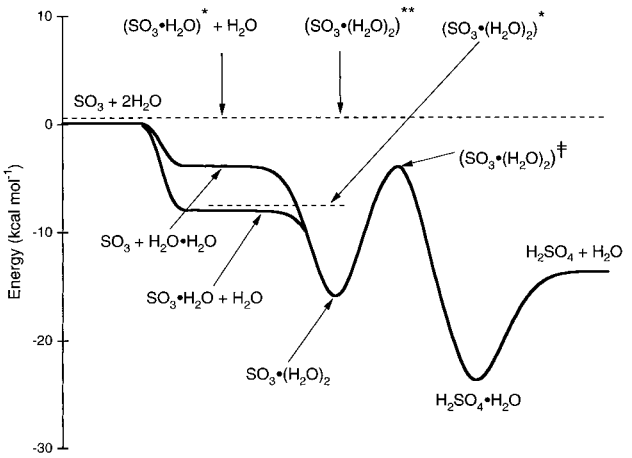

Figure 9. Reaction coordinate diagram for the $SO_3 + H_2O$ system illustrating the potential role of excited intermediates in the reaction mechanism. Competition between the forward and reverse pathways from the excited dihydrate complex may be strongly temperature dependent. Approximate potential energy values are from ref 18. Dashed lines represent the thermal energy of the system.

barrier height calculation is less reliable than the calculation of the energies of the various intermediates (Morukuma, personal communication), and hence, it appears plausible that the barrier height in question is smaller. The estimated barrier height for the reaction between $H_2O{\cdot}H_2O$ and SO_3 (reaction R6a) is practically zero; however, as mentioned above, the stability of the water dimer is sufficiently smaller than that of the $SO_3{\cdot}H_2O$ adduct to make this alternative mechanism less likely.

Yet another possibility is illustrated in Figure 9. It involves reaction of $(SO_3{\cdot}H_2O)^*$, the excited SO_3 adduct, with another water molecule to yield a dihydrate intermediate $(SO_3{\cdot}(H_2O)_2)^{**}$ with enough energy to surmount the barrier to form the six-member transition-state complex. By use of arguments similar to those described above for complex-mode reactions, such a mechanism could explain, at least in principle, the observed large negative activation energy. The third-order rate constant has a value in the range $10^{-33}-10^{-30}$ cm^6 molecule^{-2} s^{-1} (see Figure 5), fast enough for two water molecules to add to SO_3 before deactivation. On the other hand, this rate constant was observed to be pressure independent over the range of pressures investigated, whereas we would expect such a termolecular complex-mode mechanism to yield a pressure dependent third-order rate constant, unless the high-pressure limiting value is already reached at the low-pressure end of the range.

Lovejoy et al.[21] favored a reaction mechanism primarily involving the SO_3 adduct, that is, reaction R7a; however, these authors suggested that the $\sim$5 kcal mol^{-1} unaccounted for temperature dependence (13−8 kcal mol^{-1}) could be attributed mainly to uncertainties in the computed bond energies for the adduct. We believe, though, that it is unlikely that the theoretical ΔH value is in error by such a large amount. Furthermore, if the adduct binding energy were to be indeed $\sim$13.0 kcal mol^{-1}, a very large fraction (>50%) of the SO_3 in their low-temperature experiment would exist in adduct form, and the measured loss rate of SO_3 would be nearly first order in water vapor, not second order, as measured.

Atmospheric Implications

The goal of this work has been to provide improved kinetic data concerning H_2SO_4 production via reaction of SO_3 with water. Although the detailed homogeneous gas-phase reaction mechanism is still not yet fully understood, the water vapor, temperature, and total pressure dependence can be used to estimate the atmospheric lifetime of SO_3 and predict its fate in the atmosphere. In addition to its gas-phase reactivity, we can also use the results of our measurements characterizing the heterogeneous loss of SO_3 on $H_2SO_4-H_2O$ surfaces to estimate the competition between gas-phase SO_3 loss versus heterogeneous loss on atmospheric aerosols.

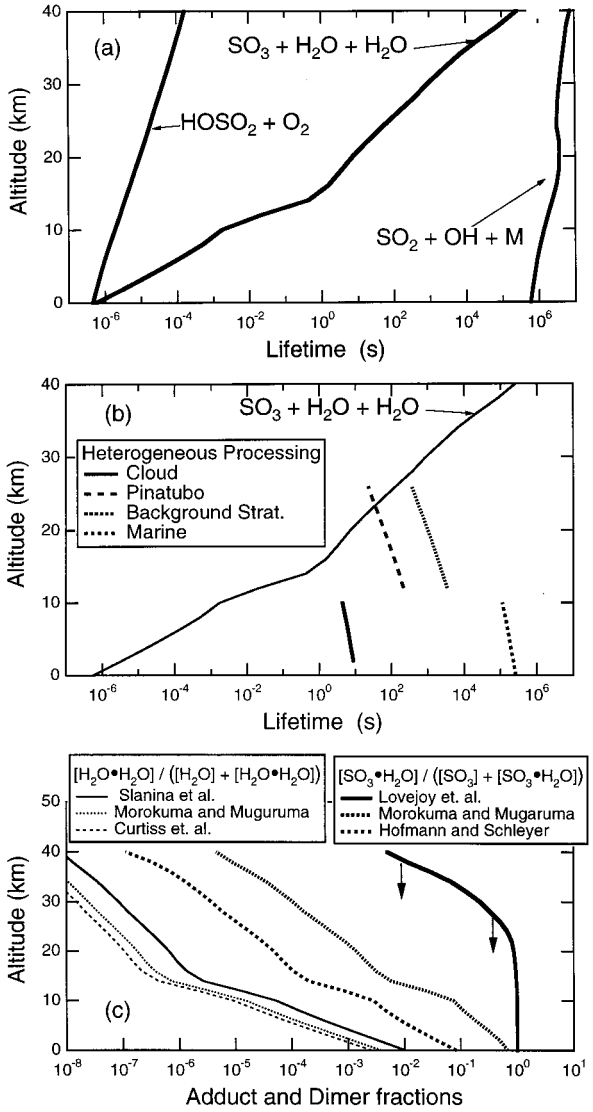

Figure 10. Gas-phase sulfur oxidation lifetimes for reactions R1−R3 (a). $SO_2 + OH + M$ is rate-limiting process in the overall gas-phase sulfuric acid formation process. Competition between gas phase and heterogeneous SO_3 loss is shown in part b for several representative atmospheric aerosol loadings. In a volcanically perturbed stratosphere, SO_3 scavenging by sulfate aerosol may compete with gas-phase reactivity. Calculated equilibrium fractions of water dimer and $SO_3{\cdot}H_2O$ adduct expected in the atmosphere as a function of altitude are shown in part c.

When considering sulfuric acid formation from gas-phase oxidation of SO_2 (reactions R1−R3), reaction R1 can be shown to be the rate-determining step in the troposphere and much of the stratosphere. The reaction of the $HOSO_2$ intermediate with O_2 (reaction R2) is much faster under atmospheric conditions, while the low concentration of atmospheric OH (generally $<10^7$ cm^{-3}) guarantees that reaction R1 governs the rate of SO_3 formation (from SO_2) and subsequent H_2SO_4 production. This is shown in Figure 10a, which plots the estimated lifetimes for SO_2, $HOSO_2$, and SO_3 as a function of altitude in the atmosphere. In this calculation we have assumed the vertical profiles for water vapor from measurements by Oltmans and

Hoffmann[44] and total pressure, temperature, and representative OH profiles from DeMore et al.[45] The pressure dependent reaction rate for R1 and the rate for R2 is the recommended value from DeMore et al.,[45] and the rate for R3 is from this work. Assuming a constant SO_2 mixing ratio of 1 ppb in the atmosphere, the lifetimes shown in Figure 10a indicate that the steady-state SO_3 concentration produced via reactions R1 and R2 will be low, ranging from ~0.1 molecule cm^{-3} at low altitude to $\sim 10^5$ molecule cm^{-3} at 30 km. Steady-state SO_3 concentrations may be 3−4 orders of magnitude larger in the plume of an aircraft exhaust due to the high S(IV) content typical of aircraft fuel and due to high oxidation rates in the combustor turbine flow and exhaust plume.[46] In the volcanically perturbed atmosphere steady-state SO_3 concentrations can be a factor of 10 or more higher than in the unperturbed atmosphere.[47]

When considering the atmospheric lifetime of SO_3, one must also account for possible heterogeneous losses in addition to the gas-phase loss process presented above. The results of our wall loss studies have indicated that the reaction probability of SO_3 on $H_2SO_4-H_2O$ surfaces is at or near unity. Therefore, the heterogeneous lifetime, τ_h, of SO_3 can be estimated by gas-phase diffusion of SO_3 to the aerosol surface[48]

$$\tau_h = \frac{r_{avg}^2}{3D_g L_c}$$

where r_{avg} is an average particle radius (cm), D_g is the gas-phase diffusion coefficient ($cm^2\ s^{-1}$), and L_c is the condensed-phase volume mixing ratio (particle volume/air volume). This expression ignores the detailed aerosol size distribution that can influence the heterogeneous kinetics under certain circumstances but is useful as an order of magnitude estimate using only these three parameters. The loss of SO_3 onto condensed-phase surfaces is considered for several cases of atmospheric aerosols. Tropospheric clouds ($r_{avg} = 10\ \mu m$; $L_c = 3 \times 10^{-7}$), marine aerosol ($r_{avg} = 10\ \mu m$; $L_c = 1 \times 10^{-11}$), background stratospheric aerosol ($r_{avg} = 0.2$; $L_c = 3 \times 10^{-14}$), and volcanically perturbed (Mt Pinatubo) stratospheric aerosol ($r_{avg} = 0.1\ \mu m$; $L_c = 3 \times 10^{-12}$). The gas diffusion coefficient was calculated from $D_g = D_p/P(T/298)^{1.89}$ where D_p is 95 Torr $cm^2\ s^{-1}$ and P is the total pressure in Torr. The temperature dependence of D_g is taken from ref 31, and the pressures used are from ref 45. By use of these relations, Figure 10b plots the heterogeneous SO_3 lifetime for each of the above aerosol cases. Replotted in the figure for comparison is the SO_3 lifetime due to gas-phase reaction with water vapor (from Figure 10a). It is clear that in the troposphere heterogeneous reaction cannot compete with the gas-phase process because of the relatively large water vapor concentrations. However, as the water vapor concentration drops with increasing altitude (to ~5 ppmv) the heterogeneous pathway becomes a more efficient process for converting SO_3 to sulfuric acid. This is particularly true in the volcanically perturbed stratosphere where heterogeneous processing may actually compete with gas-phase processing.

The slowing of the homogeneous reaction with altitude is due to the fact that the cooler temperatures found at higher altitudes, which promote adduct and dimer formation, cannot overcome the decrease in both water vapor concentration and total pressure that inhibit adduct and dimer formation. Equilibrium fractions of the water dimer $[H_2O{\cdot}H_2O]/([H_2O] + [H_2O{\cdot}H_2O])$ and the $SO_3{\cdot}H_2O$ adduct $[SO_3{\cdot}H_2O]/([SO_3] + [SO_3{\cdot}H_2O])$ are plotted in Figure 10c as a function of altitude using the data from Tables 1 and 2 and from refs 44 and 45. The water dimer and adduct fractions drop off rapidly with altitude because of decreasing water vapor partial pressure.

Summary

In this paper we have reported the temperature and pressure dependence of the gas-phase reaction of SO_3 with water vapor. The results presented here extend our earlier study over a wider temperature and pressure range and confirm our initial observation that SO_3 reactivity is second order with respect to water vapor concentration. The subject reaction has a strong negative temperature dependence (−13.5 kcal mol^{-1}) and no significant pressure dependence over the range 100−760 Torr N_2. Based on the data from this study, the details of the overall reaction mechanism cannot be fully resolved. However, it probably involves the $SO_3{\cdot}H_2O$ adduct and possibly the water dimer and can be considered a complex-mode reaction. Finally, we have also reported on the heterogeneous reactivity of SO_3 on aqueous sulfuric acid surfaces characteristic of sulfuric acid aerosols and found the reaction coefficient to be near unity, but on dry surfaces and/or fuming H_2SO_4 the reaction coefficient is negligibly small.

Acknowledgment. Financial support for this work was provided by the National Aeronautics and Space Administration's Atmospheric Effects of Aircraft Program under Contract 960501 from the Jet Propulsion Laboratory and the Air Force Phillips Laboratory/Geophysics Directorate under Contract NAS1-19949 from the NASA Langley Research Center. We thank A. A Viggiano for assistance on the ion−molecule detection schemes. U. Pöschl thanks the Austrian Science Foundation for financial support.

References and Notes

(1) Castleman, A. W.; Davis, R. E.; Munkelwitz, H. R.; Tang, I. N.; Wood, W. P. *Int. J. Chem. Kinet. Symp.* **1975**, *1*, 629.
(2) Stockwell, W. R.; Calvert, J. G. *Atmos. Environ.* **1983**, *17*, 2231.
(3) Hoffmann, D. J.; Solomon, S. *J. Geophys. Res.* **1989**, *94*, 5029.
(4) McMormick, M. P.; Thomason, L. W.; Trepte, C. R. *Nature* **1995**, *373*, 399.
(5) Charlson, R. J.; Schwartz, S. E.; Hales, J. M.; Cess, R. D.; Coakley, J. A., Jr.; Hansen, J. E.; Hofman, D. J. *Science* **1992**, *255*, 423.
(6) Miake-Lye, R. C.; Brown, R. C.; Anderson, M. R.; Kolb, C. E. *Proceedings of Impact of Emissions from Aircraft and Spacecraft on the Upper Atmosphere*, Report No. 94-06; Schumann, U., Wurzel, D., Eds.; German Aerospace Res. Est. (DLR): Cologne, 1994.
(7) Zhao, J.; Turco, R. P. *J. Aerosol Sci.* **1995**, *26*, 779.
(8) Bandy, A. R.; Scott, D. L.; Blomquist, B. W.; Chen, S. M.; Thornton, D. C. *Geophys. Res. Lett.* **1992**, *19*, 1125.
(9) Lin, X.; Chameides, W. L. *Geophys. Res. Lett.* **1993**, *20*, 579.
(10) Goodeve, C. F.; Eastman, A. S.; Dooley, A. *Trans. Faraday Soc.* **1937**, *30*, 1127.
(11) Holland, P. M.; Castleman, A. W., Jr. *Chem. Phys. Lett.* **1978**, *56*, 511.
(12) Chen, T. S.; Moore-Plummer, P. L. *J. Phys. Chem.* **1985**, *89*, 3689.
(13) Wang, X.; Jin, Y. G.; Suto, M.; Lee, L. C. *J. Chem. Phys.* **1988**, *89*, 4853.
(14) Reiner, T. H.; Arnold, F. *Geophys. Res. Lett.* **1993**, *20*, 2659.
(15) Reiner, T. H.; Arnold, F. *J. Chem Phys.* **1994**, *101*, 7399.
(16) Hofmann, M.; Schleyer, P. *J. Am. Chem. Soc.* **1994**, *116*, 4947.
(17) Kolb, C. E.; Jayne, J. T.; Worsnop, D. R.; Molina, M.; Meads, R. F.; Viggiano, A. A. *J. Am. Chem. Soc.* **1994**, *116*, 10314.
(18) Morokuma, K.; Murguruma, C. *J. Am. Chem. Soc.* **1994**, *116*, 10316.
(19) Bondeybey, V. E.; English, J. H. *J. Mol. Spectrosc.* **1985** *109*, 221.
(20) Phillips, J. A.; Canagaratna, M.; Goodfriend, H.; Leopold, K. R. *J. Phys. Chem.* **1995**, *99*, 501.
(21) Lovejoy, E. R.; Hanson, D. R.; Huey, G. *J. Phys. Chem.* **1996**, *100* (19), 911.
(22) Seeley, J. V.; Jayne, J. T.; Molina, M. J. *Int. J. Chem. Kinet.* **1993**, *25*, 571.
(23) Seeley, J. V.; Jayne, J. T.; Molina, M. J. *J. Phys. Chem.* **1996**, *100*, 4019.
(24) Seeley, J. V. Ph.D. Thesis, Massachusetts Institute of Technology, Cambridge, MA, 1994.

(25) The water vapor concentration in the flow reactor was determined using the following expressions

$$[H_2O] = \frac{F_w}{F_t + F_w}\frac{N_A P_T}{RT}$$

$$F_w = \frac{P_{H2O}}{P_B - P_{H2O}}F_B$$

where F_T = total N_2 flow through the reactor, F_B = N_2 carrier flow through the bubbler, P_T = total reactor pressure, P_B = total bubbler pressure, P_{H2O} = equilibrium water vapor pressure, N_A = Avogadro's number, R = gas constant, T = temperature.

(26) Nickless, G. *Inorganic Sulfur Chemistry*; Elsevier: London, 1968.
(27) Miller, T. M.; Viggiano, A. A.; Arnold, S. T.; Jayne, J. T. *J. Chem. Phys.* **1995**, *102*, 6021.
(28) Arnold, S. T.; Morris, R. A.; Viggiano, A. A.; Jayne, J. T. *J. Geophys. Res.* **1995**, *100* (14), 141.
(29) Viggiano, A. A.Phillips Laboratory, Geophysics Directorate, Ionospheric Division (GPID), Hanscom Air Force Base, Massachusetts. Private communication.
(30) Taleb, D. E.; Ponche, J. L.; Mirabel, P. *J. Geophys. Res.* **1996**, *101*, 25967.
(31) Ferguson, E. E.; Fehsenfeld, F. C.; Schmeltekopl, A. L. *Adv. At. Mol. Phys.* **1969**, *5*, 1.
(32) Key, R. J.; Miller T. H.; Jefferson, T. H. CHEMKIN: *A chemical kinetics code package*; Sandia Laboratories: Albuquerque, NM, 1989.
(33) Monchick, L.; Mason, E. A. *J. Chem. Phys.* **1961**, *35*, 1676. Mason, E. A.; Monchick, L. *J. Chem Phys.* **1962**, *36*, 2746.
(34) Lovejoy, E. R.; Hanson, D. R. *J. Phys. Chem.* **1996**, *100*, 4459.
(35) Brown, R. L. *J. Res. Natl. Bur. Stand.* **1978**, *83*, 1.
(36) Gmitro, J. I.; Vermeulen, T. *AIChE J.* **1964**, *10*, 740.
(37) *Encyclopedia of Chemical Technology*, 3rd ed.; Kirk, R. E., Othmer, D. E., Eds.; Wiley: New York, 1983; Vol. 22.
(38) Lovejoy, E. R.; Hanson, D. R. *J. Phys. Chem.* **1995**, *99*, 2080.
(39) Fried, A.; Henry, B. E.; Calvert, J. G.; Mozurkewich, M. *J. Geophys. Res.* **1994**, *99*, 3517.
(40) Slanina, Z.; Crifo, J.-F. *Thermochim. Acta* **1991**, *181*, 109.
(41) Curtiss, L. A.; Fruip, D. J.; Blander, M. *J. Chem. Phys.* **1979**, *71*, 2703.
(42) Munoz-Caro, C.; Nino, A. *J. Phys. Chem.* **1997**, *101*, 4128.
(43) Troe, J. *J. Chem. Soc., Faraday Trans.* **1994**, *90*, 2303.
(44) Oltmanns, S. J.; Hofmann, D. J. *Nature* **1995**, *374*, 146.
(45) DeMore, D. B.; Sander, S. P.; Golden, D. M.; Hampson, R. F.; Kurylo, M. J.; Howard, C. J.; Ravishankara, A. R.; Kolb, C. E.; Molina, M. J. Chemical kinetics and photochemical data for use in stratospheric modeling. JPL Publication 94-26; Jet Propulsion Laboratory: Pasadena, CA, 1994.
(46) Brown, R. C.; Anderson, M. R.; Miake-Lye, R. C.; Kolb, C. E.; Sorokin, A. A.; Buriko, Y. Y. *Geophys. Res. Lett.* **1996**, *23*, 3603.
(47) Mankin, W. G.; Coffey, M. T.; Goldman, A. *Geophys. Res. Lett.* **1992**, *19*, 179.
(48) Kolb, C. E.; Worsnop, D. R.; Zahniser, M. S.; Davidovits, P.; Keyser, L. F.; Leu, M.-T.; Molina, M. J.; Hanson, D. R.; Ravishankara, A. R.; Williams, L. R.; Tolbert, M. A. Laboratory Studies of Atmospheric Heterogeneous Chemistry. In *Progress and problems in atmospheric chemistry*; Barker, J. R., Ed.; Advanced Series in Physical Chemistry; World Scientific Publishing Co.: River Edge, NJ, 1995; Vol 3, p 771.